https://doi.org/10.5194/tc-2023-16
Preprint. Discussion started: 21 February 2023

The Cryosphere Discussions

Drivers and rarity of the strong 1940s westerly wind event over the Amundsen Sea, West Antarctica

Gemma K. O'Connor[1], Paul R. Holland[2], Eric J. Steig[1,3], Pierre Dutrieux[2], Gregory J. Hakim[3]

[1]Department of Earth and Space Sciences, University of Washington, Seattle, WA, USA
[2]British Antarctic Survey, Cambridge, UK
[3]Department of Atmospheric Sciences, University of Washington, Seattle, WA, USA

Correspondence to: Gemma K. O'Connor (goconnor@uw.edu)

Abstract. Glaciers in the Amundsen Sea Embayment of West Antarctica are rapidly retreating and contributing to sea level rise. Ice loss is occurring primarily via exposure to warm ocean water, which varies in response to local wind variability. There is evidence that retreat was initiated in the mid-20th century, but the perturbation that may have triggered retreat remains unknown. A leading hypothesis is that large pressure and wind anomalies in the 1940s drove exceptionally strong oceanic ice-shelf melting. However, the characteristics, drivers, and rarity of the atmospheric event remain poorly constrained. We investigate the 1940s atmospheric event using paleoclimate reconstructions and climate model simulations. The reconstructions show that large westerly wind anomalies occurred from ~1938-1942, a combined response to the very large El Niño event from 1940-1942 and other variability beginning years earlier. Climate model simulations provide evidence that events of similar magnitude and duration are unusual but may have occurred tens to hundreds of times throughout the Holocene. Our results suggest that the 1940s westerly event is unlikely to have been exceptional enough to be the sole explanation for the initiation of Amundsen Sea glacier retreat. Naturally arising variability in ocean conditions prior to the 1940s, or anthropogenically driven trends since the 1940s, may be needed to explain the onset of retreat in West Antarctica.

1 Introduction

Glaciers in the Amundsen Sea Embayment (ASE) of West Antarctica are rapidly retreating, contributing significantly to global sea level rise. Ice loss is occurring via ocean-driven melting of the ice shelves that buttress the glaciers, causing the glaciers to retreat at an accelerating rate (Pritchard et al., 2012; Shepherd et al., 2019; Smith et al., 2020). There is evidence that these glaciers have been relatively stable for the last ~10,000 years (Larter et al., 2014), which implies that a change in ocean circulation, and a corresponding increase in heat delivery to the ice shelves, must have occurred to initiate the current stage of retreat. However, direct observations of glaciological, oceanic, and atmospheric conditions in the ASE only span recent decades (i.e., 1979 or later), making it difficult to assess this idea (e.g., Bracegirdle, 2013; Dutrieux et al., 2014; Jenkins et al., 2018; Smith et al., 2020; Alley et al., 2021; Wåhlin et al., 2021).

There is evidence for a link between the poleward transport of the warm Circumpolar Deep Water (CDW) that is melting the ice shelves and westerly winds over the ASE continental shelf break region (Thoma et al., 2008; Dutrieux

https://doi.org/10.5194/tc-2023-16
Preprint. Discussion started: 21 February 2023

et al., 2014; Jenkins et al., 2016). Previous studies based on climate models and regional ocean models suggest that a trend toward stronger westerly conditions over the 20th century would increase the amount of warm CDW that is transported toward the glaciers, causing increased ice-shelf melt (Holland et al., 2019; Naughten et al., 2022). However, proxy-constrained reconstructions of wind conditions in the ASE show no evidence of a westerly trend at the shelf break; instead, the average trend over the 20th century in this region has been weakly easterly, associated with a deepening of the Amundsen Sea Low (O'Connor et al., 2021a; Dalaiden et al., 2021; Holland et al., 2022).

Previous studies have suggested that, rather than a trend, an extremely large climate anomaly around 1940 is a candidate event for initiating ice retreat. Schneider and Steig (2008) used a network of ice core data to show that a warming occurred in West Antarctica from ~1936 to 1945, likely accompanied by a high sea level pressure anomaly over the Amundsen Sea. They attributed this to the very strong 1940-42 El Niño event because of the similar timing and the known teleconnection between atmospheric circulation in the Amundsen Sea and tropical Pacific climate variability (Lachlan-Cope and Connolley, 2006; Ding et al., 2011). Steig et al. (2012, 2013) showed that similar West Antarctic warming events are consistent with enhanced westerlies at the shelf break, and suggested that the 1940 warming was associated with enhanced westerlies and thus enhanced transport of warm CDW. These studies are limited by a lack of reliable pressure and wind data in this region before the 1980s, leaving large uncertainties in the atmospheric circulation patterns over the Amundsen Sea around 1940. There is additional evidence from sediment cores that show the 1940s is a notable period for the glaciers, as Pine Island Glacier may have started to retreat at this time (Smith et al., 2017). Together, these results suggest that glacier retreat was initiated by an exceptional wind-driven anomaly in ocean circulation and ice-shelf melting that occurred around 1940.

Until recently, evaluation of the idea that atmospheric circulation changes in the 1940s were a critical trigger for glacier change was hindered by a lack of observational constraints in the ASE region. Recent developments in proxy data assimilation have enabled more reliable reconstructions of pressure and winds in the Amundsen Sea throughout the full 20th century (O'Connor et al., 2021a, Dalaiden et al., 2021). Holland et al. (2022) used reconstructed pressure and winds from O'Connor et al. (2021a) to evaluate the relative influences of anthropogenic forcing and internal climate variability on trends in the ASE. They found that internal variability may have played a large role in opposing the effects of anthropogenic forcing. Rather than a century-scale trend suggested by poorly constrained climate model simulations, a prominent feature of the proxy reconstructions over the Amundsen Sea is a large westerly anomaly at the shelf break during the 1940s, consistent with the suggestion that this may have been a key event for initiating glacier retreat.

In this study, we use annually resolved proxy reconstructions and climate model simulations of surface pressure and winds to further investigate the hypothesis that a large atmospheric event in the ASE around 1940 forced the ocean-induced changes responsible for triggering glacier retreat. Specifically, we investigate the significance of the atmospheric component of the hypothesis. Was the atmospheric event unprecedented in the Holocene, providing a possible explanation for the initiation of glacier retreat after millennia of stability? Or was it a relatively common

https://doi.org/10.5194/tc-2023-16
Preprint. Discussion started: 21 February 2023

75 event, perhaps superimposed on other glaciological or oceanic conditions favorable for initiating retreat? To investigate the significance of the atmospheric event, we first evaluate the timing and magnitude of the pressure and wind anomalies in the ASE around 1940, using two different proxy reconstructions to assess uncertainty. Next, we use proxy data assimilation to generate new reconstructions with certain proxy types withheld, allowing us to evaluate the drivers of the reconstructed ASE anomalies. Finally, we evaluate whether the anomalies are rare in the context of 80 10,000 years of simulated internal climate variability, providing an estimate for the exceptionality of the 1940s atmospheric event relative to the Holocene.

2 Methods

85 2.1 Paleoclimate reconstructions

We use paleoclimate reconstructions to characterize anomalies in sea level pressure (SLP) and surface wind (U_S) in the ASE shelf break region (70-72°S, 102-115°W). Instrumental reanalysis products such as 20CR (Slivinski et al., 2019) and the Fogt et al. (2019) pressure reconstruction include the 1940s but are considered unreliable in the 90 Amundsen Sea region given the sparsity of relevant instrumental observations (Fogt et al., 2019; Wohland et al., 2019; Holland et al., 2022). We therefore focus only on reconstructions that use proxy data, as consistent coverage from relevant regions throughout the full 20th century is available. This includes multiple, precisely dated ice core records from the relevant West Antarctic region (e.g., Steig et al., 2013; Thomas et al., 2017; PAGES2k consortium 2017) and coral records from the critical tropical Pacific region (e.g., Cobb 2002; Sanchez et al., 2020; 2021; PAGES2k 95 consortium 2017).

We use two paleoclimate reconstructions in this study. The first is a proxy-based reconstruction from O'Connor et al. (2021a), which we refer to as the "natural-prior reconstruction". This gridded 20th century reconstruction (1° spatial resolution, available from 1900 to 2005) spans the Southern Ocean and includes data from a global database of proxy 100 records. It was generated using the Community Earth System Model 1 (CESM1) Last Millennium climate model simulation (Brady et al. 2019), without anthropogenic forcing, as the data assimilation prior. The prior is used as the initial estimate of the climate state and provides the estimate of climate covariance patterns. Four other proxy reconstructions of 20th century atmospheric circulation are available in this region, which use different techniques and proxy databases (Dalaiden et al., 2021) or different climate model priors (O'Connor et al., 2021a), but produce very 105 similar results. The natural-prior reconstruction from O'Connor et al. (2021a) shows the greatest skill, especially for zonal winds, in the key ASE continental shelf break region (Figs. 1, A1). Skill is based on correlation and coefficient of efficiency (a measure of signal amplitude and bias) relative to modern ERA5 reanalysis winds (Hersbach et al., 2020; data are constrained by satellite infrared sounding observations) for the overlapping period of 1979 to 2005.

https://doi.org/10.5194/tc-2023-16
Preprint. Discussion started: 21 February 2023

The Cryosphere
Discussions
Open Access
EGU

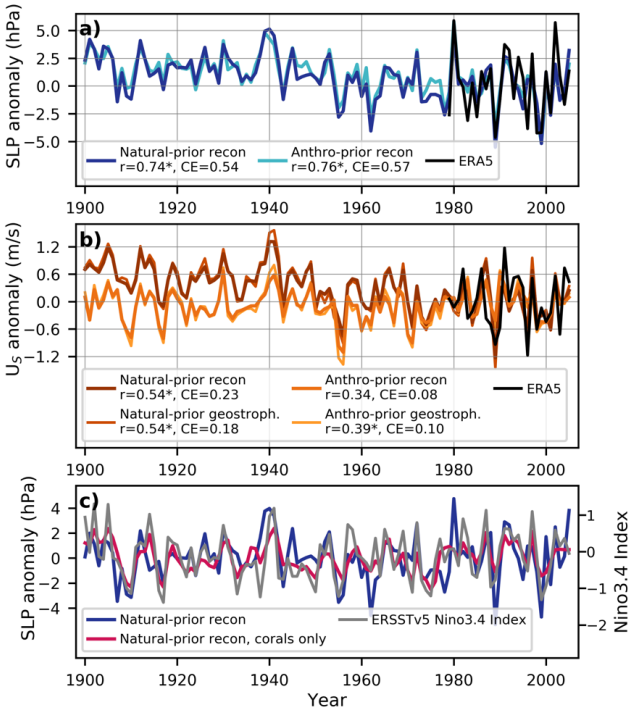

Figure 1. (a) Reconstructed SLP anomalies in the natural-prior reconstruction ensemble mean, anthro-prior reconstruction ensemble mean, and ERA5 averaged over the continental shelf break box (location shown in Fig. 3). Correlation (r) and coefficient of efficiency (CE; values > 0 are skillful) values between each reconstruction and ERA5 from 1979 to 2005 are shown in the legend. An asterisk is given next to the correlation value if it is significant with 95% confidence. (b) Same as in (a), but for U_S. Geostrophic winds generated using the SLP reconstructions are also shown. (c) SLP in the natural-prior reconstruction with all proxies assimilated and with only coral records assimilated. Also shown is the Nino3.4 Index from ERSSTv5. All timeseries in panel (c) are detrended. Anomaly reference period for all panels is 1979-2005.

While the natural-prior reconstruction shows the greatest agreement with ERA5 in terms of interannual variability, the relatively brief 27-year verification period precludes evaluation of the reliability of multi-decadal or century-scale trends in the reconstructions. Evaluation of trends is particularly important for analyzing the 1940s, as the magnitude of the 1940s wind anomalies is sensitive to the reconstructed trends (Figs. 1, A1). The reconstructions generated with naturally forced climate model priors show easterly trends, while those that include anthropogenic forcing in the climate model prior show negligible trends – consistent with previous studies that show that greenhouse gases and ozone induce westerly trends (Arblaster and Meehl, 2006; Thompson et al., 2011; Bracegirdle et al., 2014; 2020; Goyal et al., 2021) opposing the naturally induced easterly trends (Holland et al., 2022). As a result of the uncertainty associated with the reconstructed trends, we also evaluate the O'Connor et al. (2021a) reconstruction that uses a climate-model prior with historical anthropogenic forcing; we refer to this as the "anthro-prior reconstruction". The prior for this reconstruction comes from the CESM1 tropical Pacific "pacemaker" ensemble of 20 simulations (Schneider and Deser, 2018). The anthro-prior reconstruction shows the lowest magnitude during the 1940s (Figs. 1,

https://doi.org/10.5194/tc-2023-16
Preprint. Discussion started: 21 February 2023

A1). Together with the natural-prior reconstruction, this makes it ideal for evaluating the full range of uncertainties among the available reconstructions.

The SLP reconstructions are more skillful than the wind reconstructions (as evaluated against ERA5), so we consider both the winds reconstructed by O'Connor et al. (2021a) and geostrophic winds calculated using the SLP reconstructions, following the approach used in Holland et al. (2022). This is especially useful for the anthro-prior reconstruction, which shows increased skill when we use geostrophic winds rather than the directly reconstructed winds (Holland et al., 2022; Fig. 1).

Specifics on how the two reconstructions were generated can be found in O'Connor et al. (2021a), but we emphasize two key qualities: (1) the climate-model prior is used as an "offline" prior (the same initial guess is used every year), so all of the variability in the reconstruction is generated from the proxy data, rather than from the climate model simulation; (2) the influence of each proxy record on the reconstructed climate in a given location depends on the covariance structures in the climate model prior (this explains the differences in the two O'Connor et al. (2021a) reconstructions used in this study).

The reconstructions each include an ensemble of 100 members, which reflects the uncertainty associated with each reconstruction (Fig. 2a/b). We use the reconstruction ensemble mean to characterize the 1940s event (Fig. 1) and evaluate the drivers of the event (Figs. 3, 4). For evaluating the rarity of the event, we compare the amplitude of the 1940s event to thousands of years of simulated internal climate variability; this result is sensitive to the precise amplitude of the 1940s anomalies, so we use all ensemble members in the reconstruction to account for uncertainty in this calculation. The reconstruction ensemble reflects different random draws from the climate model priors, so the members only differ by their means (Fig. 2a/b). The temporal variance is the same in each member because the temporal variance is derived from the proxy data, and each member contains information from the same proxy database. We generate an ensemble of independent members by removing the assumption that each datapoint is autocorrelated in time; we refer to this as "scrambling" the ensemble members (Fig. 2c/d). This has two purposes: (1) each scrambled member becomes a unique realization, allowing us to conduct a rigorous test for uncertainty, and (2) the variance of each scrambled member becomes larger (even though the ensemble variance is the same, as shown in Figs. 2a-d). The larger variance in the scrambled members allows us to compare the reconstructed members to individual members in climate model simulations (more details in the following section), as the variances between these data products is now similar (Fig. 2e/f). More details on the scrambling methods and reconstruction dataset processing can be found in Section 4.1 and Appendix A.

https://doi.org/10.5194/tc-2023-16
Preprint. Discussion started: 21 February 2023

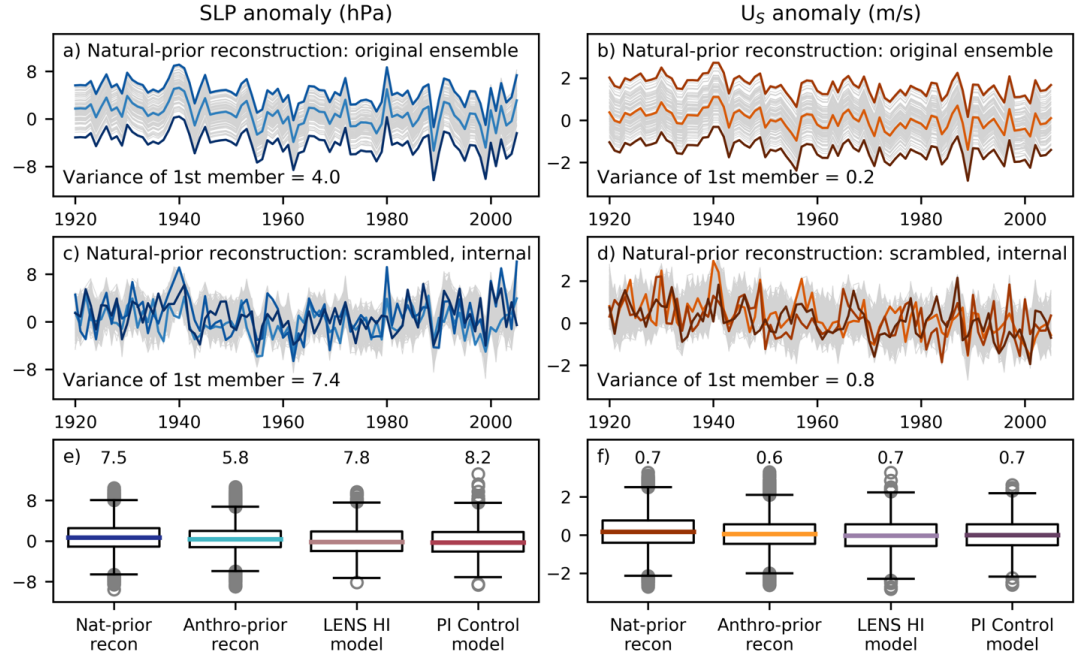

Figure 2. Reconstructed and simulated anomalies in SLP (left panels) and U_S (right panels). (a, b) The original 100 ensemble members in the natural-prior reconstruction. (c, d) The 300 ensemble members in the natural-prior reconstruction ensemble, after scrambling the members and isolating the internal component. All timeseries are in anomalies relative to 1961 to 1990. Only three members in each ensemble are plotted in color to highlight the variability of each member (the members containing the minimum, maximum, and median value during 1940); all other members are plotted in gray. (e, f) Box and whisker plots of all data used to calculate the rarity of the 1940s event: two reconstructions (using the internal component of the scrambled ensembles) and two climate model simulations (the internal component of the LENS historical ensemble (LENS HI) and the Preindustrial Control simulation (PI Control)). The colored lines show the medians, the boxes show the inner quartiles, and gray circles show outliers. The variances of each dataset are shown above each boxplot. The corresponding time series of all datasets are shown in Fig. A3.

To investigate the drivers of the 1940s event, we generate new single-proxy reconstructions, in which we assimilate only ice cores or only coral records. These provide an important measure of the role of local (Antarctic) *vs*. remote (tropical) proxies in influencing the results. We follow the methods developed by Hakim et al. (2016) and adapted by O'Connor et al. (2021a) to generate these reconstructions.

2.2 Climate model simulations

We evaluate the rarity of the 1940s pressure and wind event by comparing the 1940s anomalies (as characterized by the scrambled reconstruction ensembles) to thousands of years of simulated internal climate variability. Specifically, we count the occurrences of similar events in climate model simulations to calculate the frequency of 1940s-like

https://doi.org/10.5194/tc-2023-16
Preprint. Discussion started: 21 February 2023

events in 10kyr of natural climate variability (analogous to the Holocene). We use two sets of climate model simulations to conduct this comparison: the CESM1 preindustrial control simulation (PI Control) and the internal component of the CESM1 Large Ensemble Historical ensemble (LENS HI; "I" denotes that the influence of historical external forcing is removed and we are only considering internal variability). PI Control and LENS HI are both fully coupled and have ~1° horizontal resolution (Kay et al., 2015). The PI Control is a single simulation of 1,801 years total and contains no anthropogenic forcing. The LENS historical ensemble contains 40 simulations from 1920-2005 for a total of 3,440 years and follows historical anthropogenic forcings over the 20th century. We remove the externally forced component in the historical ensemble to ensure that both simulations reflect internal climate variability only (more details in Appendix B). We use these two sets of simulations because they have low bias in atmospheric circulation in the Amundsen Sea region relative to other climate models (Holland et al., 2019). Furthermore, the reconstructions lie within the range of states generated by LENS historical simulations (Holland et al., 2022). Additional details on the methods used for the frequency calculation can be found in section 4.1.

3 Characteristics and Drivers of the 1940s event

3.1 Event characteristics

We use the natural-prior reconstruction and the anthro-prior reconstruction ensemble means to investigate the characteristics of the anomalies around 1940 (Fig. 1). Both reconstructions show high pressure and westerly anomalies in the ASE shelf break region lasting approximately five years, from ~1938 to 1942. This demonstrates high confidence that a persistent atmospheric event occurred in the ASE at this time, consistent with previous work (Schneider and Steig, 2008; Steig et al., 2012; 2013). The spatial patterns of pressure and zonal winds reveal that the shelf-break anomalies are part of an anti-cyclonic feature centered over the South Pacific, just north of the ASE shelf break, emerging as early as 1937. This coincides with local warming patterns and is accompanied by easterly anomalies in the mid-latitude Pacific (Fig. 3).

https://doi.org/10.5194/tc-2023-16
Preprint. Discussion started: 21 February 2023

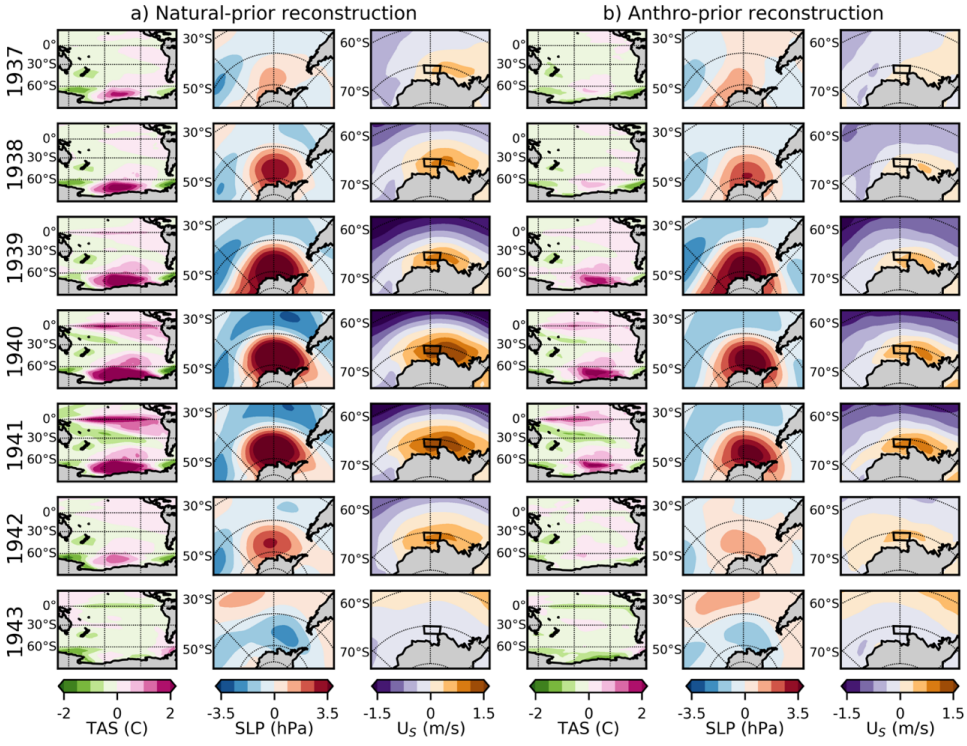

Figure 3. (a) Reconstructed anomalies in surface air temperature (TAS), SLP, and U_S in the natural-prior reconstruction (with all proxies assimilated) from the years 1937 to 1943 (the reconstruction ensemble means are shown). (b) Same as in (a) but with the anthro-prior reconstruction. Anomaly reference period is 1961-1990. The black box on the wind panel shows the Amundsen Sea Embayment (ASE) continental shelf break region.

Both reconstructions agree well with each other and show similar trends toward lower pressure over the 20th century (Fig. 1a). The SLP anomaly reaches a distinct 3-year peak from 1939 to 1941, with the greatest anomaly occurring in 1940. The natural-prior reconstruction maintains a mean anomaly of 4.9 hPa during the three peak years, and the anthro-prior reconstruction reaches a slightly lower peak of 4.3 hPa (anomalies in this section are relative to the period 1979 to 2005 for comparison to ERA5, as shown in Fig. 1). While a similar magnitude anomaly occurred in 1980, it is shorter lived and is not accompanied by a strong westerly anomaly. The 1940s SLP event is the only event in the 20th century that maintains such a large magnitude for three consecutive years (this is also true for 2-year, 4-year, or 5-year averages centered around 1940). Even if the trends in the time series are removed, the 1940 multi-year event remains an outlier relative to the rest of the 20th century. Thus, there is robust evidence from both reconstructions that the SLP anomalies that occurred around 1940 are exceptional in terms of combined magnitude and persistence.

Both reconstructions show westerly wind anomalies for at least four years from 1938 to 1942, with a distinct 2-year peak in 1940 and 1941 (Fig. 1b) – one year later and shorter than the distinct peak in SLP. The spatial pattern of SLP indicates that the westerly anomaly reaches its maximum later due to the more southward position of the high-pressure

https://doi.org/10.5194/tc-2023-16
Preprint. Discussion started: 21 February 2023

center in 1939 (Fig. 3). The natural-prior reconstruction shows a trend toward easterly conditions over the 20th century, while the anthro-prior reconstruction shows no trend (O'Connor et al., 2021a; Fig. 1b), making the 1940 to 1941 wind anomaly weaker in the anthro-prior reconstruction. The natural-prior wind reconstruction maintains a 2-year peak anomaly of 1.3 m/s from 1940 to 1942, and the anthro-prior reconstruction reaches a weaker peak of 0.5 m/s (relative to an anomaly reference period of 1979-2005). As for SLP, the 1940s wind event is the only one during the 20th century to reach such high magnitudes for two consecutive years. This statement remains true for both reconstructions if we define the wind event using its 3-year, 4-year, or 5-year magnitudes and if we remove the easterly trend. When we use geostrophic winds rather than the directly reconstructed winds, we find that the event has the same timing but greater magnitudes (Fig. 1b), and that it is still a unique event in the 20th century. In short, although the event magnitude is sensitive to the choice of reconstruction, there is robust evidence that a notable multi-year westerly anomaly occurred in the ASE shelf break region centered in 1940-41.

3.2 Drivers of the 1940s event

We compare the reconstructed ASE SLP with the Nino3.4 Index (based on the Extended Reconstructed Sea Surface Temperature dataset v5 (ERSSTv5); Huang et al., 2017), a commonly used index for measuring El Niño – Southern Oscillation variability based on sea surface temperatures in the central tropical Pacific. Our comparison over the 20th century suggests that much of the SLP variability is associated with tropical Pacific sea surface temperature variability (Fig. 1c; $r = 0.29$ and 0.23 in the natural-prior and anthro-prior reconstructions, respectively; p-values <0.05), as earlier studies have established (e.g., Lachlan-Cope & Connolley, 2006; Ding et al., 2011; Steig et al., 2012; Holland et al., 2019). Previous work has suggested that the 1940s event in the Amundsen Sea was a response to the large ~1940-42 El Niño event (Schneider and Steig, 2008; Steig et al., 2012) which was unusually persistent (Bronnimann et al., 2004). Our reconstructions are consistent with that suggestion, as they show high pressure and westerly anomalies characteristic of a classic Rossby wave train response during El Niño years. However, the reconstructions also show that the South Pacific warming and high-pressure anomalies led the onset of the 1940 El Niño by up to two years (Figs. 1c, 3), suggesting that they are not exclusively a response to tropical Pacific convection. Instead, the high pressures and shelf-break westerlies from 1938 to 1942 may be a compounded response to both tropical Pacific convection and local internal variability or teleconnections with regions other than the tropical Pacific (Li et al., 2021).

To further investigate the origin of the anomalies in the Amundsen Sea, we conduct single-proxy experiments. We generate two new types of reconstructions: one in which we assimilate only ice core records, and one in which we assimilate only coral records. We use the same proxy database, ensemble Kalman filter method, and two priors (one with natural forcing and one with anthropogenic forcing) as in O'Connor et al. (2021a). The ice-only reconstruction reveals signals captured in Antarctica (primarily West Antarctica, which has the greatest number of high-resolution ice-core records); the coral-only reconstruction highlights signals captured in the tropics (primarily the tropical Pacific). For simplicity, we present the results from the natural-prior single-proxy experiments in the main text (using the reconstruction ensemble mean), but our results are similar when we use the anthro-prior (Fig. A2). The ice-only

https://doi.org/10.5194/tc-2023-16
Preprint. Discussion started: 21 February 2023

reconstruction shows large warming, high pressure, and westerly anomalies in the Amundsen Sea starting as early as 1938 (Fig. 4). In the coral-only reconstruction, those signals do not emerge until 1940 and 1941, further indicating that the high pressure and large westerly anomalies detected in the Amundsen Sea cannot exclusively be a response to tropical Pacific variability (Figs. 1c, 4).

275

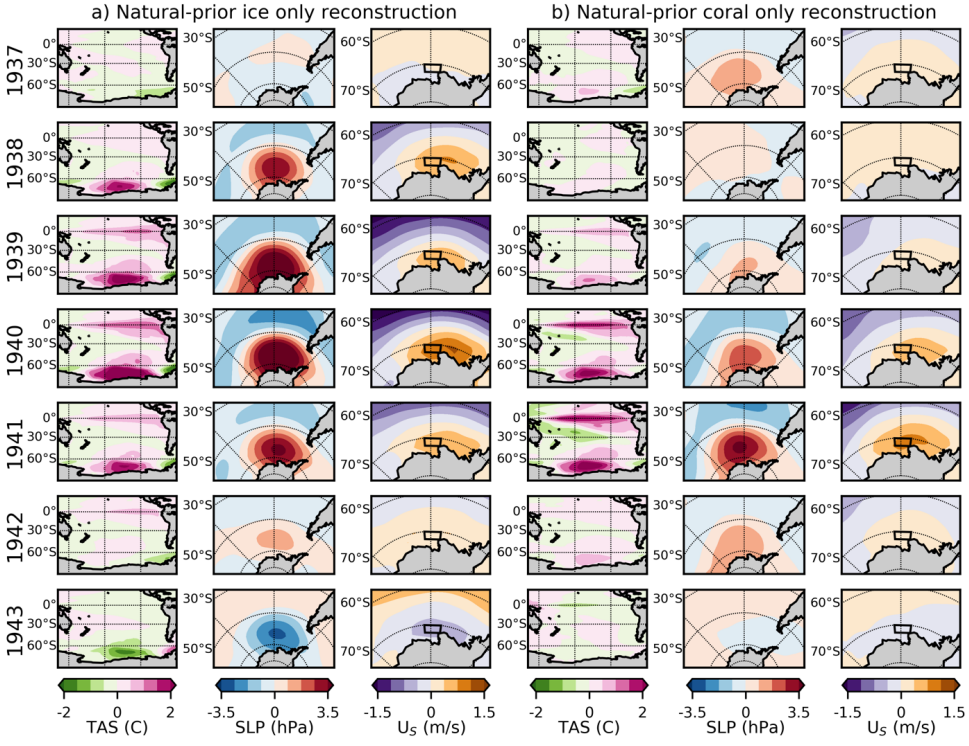

Figure 4. Same as in Fig. 3, but with the natural-prior and only ice cores assimilated (a) and only corals assimilated (b). The same figure using the anthro-prior is shown in Fig. A2.

280

It is possible, in principle, that the differences in timing of local anomalies and tropical Pacific anomalies could reflect dating uncertainty in the proxy records. However, this is unlikely: the West Antarctic ice cores have a demonstrated dating uncertainty of less than 1 year owing to the use of multiple volcanic markers of known age, and unambiguous seasonal variations in chemistry (Steig et al., 2005). Furthermore, even higher resolutions are available in tropical
285 Pacific coral records, enabling dating uncertainties of one to two months in modern corals and less than 1 year in fossil corals (Cobb, 2002; Sanchez et al., 2020; O'Connor et al., 2021b). As an additional test that does not depend on proxy data, we analyze the tropical Pacific pacemaker ensemble v1 ("PACE") – a set of 20 simulations constrained to follow tropical Pacific sea surface temperatures starting in 1920 (the same simulations used to form the prior in the anthro-prior reconstruction). The ensemble mean of the PACE simulations – which represents the response to tropical Pacific

https://doi.org/10.5194/tc-2023-16
Preprint. Discussion started: 21 February 2023

290 variability and external forcing – shows high pressures and shelf break westerlies in the ASE only in 1940 and 1941 (Fig. 5), consistent with the results from our single-proxy experiments. The individual members in the PACE ensemble represent realizations of climate variability driven by influences outside of the tropical Pacific; several members show high pressure anomalies in the Amundsen Sea and shelf break westerlies in 1938 and 1939, demonstrating that these patterns can indeed emerge even in the absence of tropical Pacific forcing (example members shown in Fig. 4). These
295 simulations bolster the results from the single-proxy reconstructions: it is unlikely that the 1940s event over the Amundsen Sea was exclusively a response to the 1940-42 El Niño. Rather, it appears likely that local variability or perhaps a response to tropical forcing from outside the Pacific (e.g., Okumura et al., 2012; Li et al., 2021), in addition to ENSO, played a significant role in producing a multi-year large-magnitude event in the ASE shelf break region.

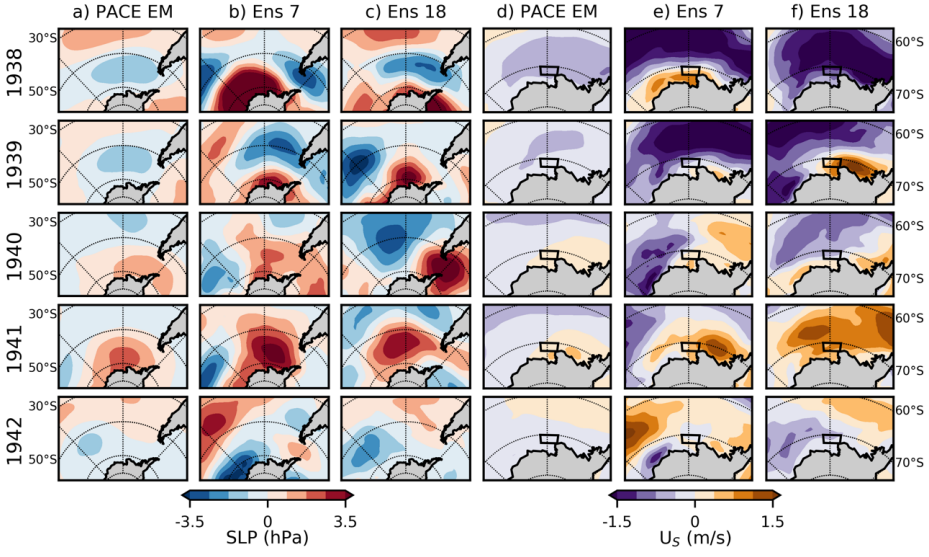

300 **Figure 5.** (a-c) Modeled SLP and (d-f) U_S anomalies from 1938 to 1942 in the tropical Pacific pacemaker ensemble of simulations ('PACE'). The ensemble mean, ensemble 7, and ensemble 18 of the PACE ensemble is shown. Anomaly reference period is 1961 to 1990.

305

4 Rarity of the 1940s event in a natural climate

The 1940s event in the ASE is notable because it is likely a combined response to both an exceptionally persistent El Niño event, and to other sources of variability occurring in preceding years. This suggests that the frequency of this
310 type of event in the ASE is not comparable to the frequency of El Niño events; it is probably much rarer. Quantifying the frequency of the 1940s ASE pressure and westerly anomalies in the context of internal climate variability is crucial for investigating the question of why glacier retreat may have started in the 1940s, as suggested by the sediment-core evidence (Smith et al., 2017). Was the ongoing ice retreat triggered solely by a very unlikely natural event in the 1940s (e.g., an event that is unprecedented in millennia)? Or was that event a relatively common occurrence that only

https://doi.org/10.5194/tc-2023-16
Preprint. Discussion started: 21 February 2023

315 triggered ice retreat in 1940 in combination with other conditions favorable for retreat? In this section, we calculate the frequency of the 1940s anomalies occurring in a natural climate by looking for similar occurrences within thousands of years of climate model simulations without anthropogenic forcing. We evaluate the statistics of these occurrences to investigate whether the 1940s event may be exceptional in the context of Holocene climate variability.

320 **4.1 Frequency calculation**

To estimate the frequency of the 1940s event, we use reconstructions to quantify the magnitude of the event and then search simulations of internal climate variability for events that meet or exceed that magnitude. We explain the details of the calculations here; the results for SLP and U_S and reviewed in sections 4.2 and 4.3, respectively.

325

To quantify the magnitude of the 1940s event, we use both the natural-prior and anthro-prior reconstructions. As described in section 2.1, we use the scrambled reconstructions ensembles to ensure that uncertainty is fully accounted for and that the variances of all datasets used in the calculation are comparable (Figs. 2e/f). As described in section 2.2, we compare the reconstructed magnitudes to internal climate variability as captured by the PI Control (a single
330 simulation without anthropogenic forcing) and LENS HI (an ensemble of historical simulations with the externally forced component – quantified as the ensemble mean of the LENS historical ensemble – removed). We process all datasets to ensure that they all reflect the internal component of climate variability and contain the same anomaly reference periods (more details in Appendix B; timeseries are shown in Fig. A3).

335 With the two reconstruction ensembles and two sets of climate model simulations, we calculate the frequency of the 1940s event in a natural climate. To go through an example of the calculation, let us use the natural-prior SLP reconstruction (using the internal component of the scrambled ensemble) to quantify the 1940s event magnitude, which we define as the 5-year mean centered on 1940 (1938 to 1942). We use the ensemble to quantify the mean magnitude and its 95% confidence interval, as shown in Fig. 6a (see the values for the 5-year window length to follow
340 this example). Next, we use the PI Control simulation to evaluate the statistics of the 5-year magnitude relative to internal climate variability. We calculate the means of all 5-year windows in the PI Control simulation of SLP, sampling with a 50% overlapping window. As a simple statistic for evaluating the significance of the reconstructed 5-year magnitude relative to internal variability, we calculate the sigma level of the magnitude, i.e. the number of standard deviations from the simulated 5-year samples (assuming Gaussian statistics; Fig. 6c). Next, we calculate the
345 frequency of the 5-year magnitude as follows: if any 5-year SLP sample from the simulation has a mean magnitude at least as great as the reconstructed 5-year magnitude, it counts as an occurrence. The total number of occurrences divided by the sample size (the number of 5-year windows in the simulation) equals the fractional probability; we multiply this probability by 10,000 to yield the frequency of the 1940s event per 10 kyr (Fig. 6c). We report the frequency per 10 kyr to serve as an analogue for the estimated number of occurrences throughout the Holocene. The
350 calculations are sensitive to the precise magnitude used to characterize the 1940s event, so we propagate the confidence intervals from the reconstructed magnitudes (Fig. 6a) throughout the sigma and frequency calculations

https://doi.org/10.5194/tc-2023-16
Preprint. Discussion started: 21 February 2023

(i.e., we repeat the calculation using the upper and lower bounds of the reconstructed magnitude; results are shown as error bars in Figs. 6c, 6e).

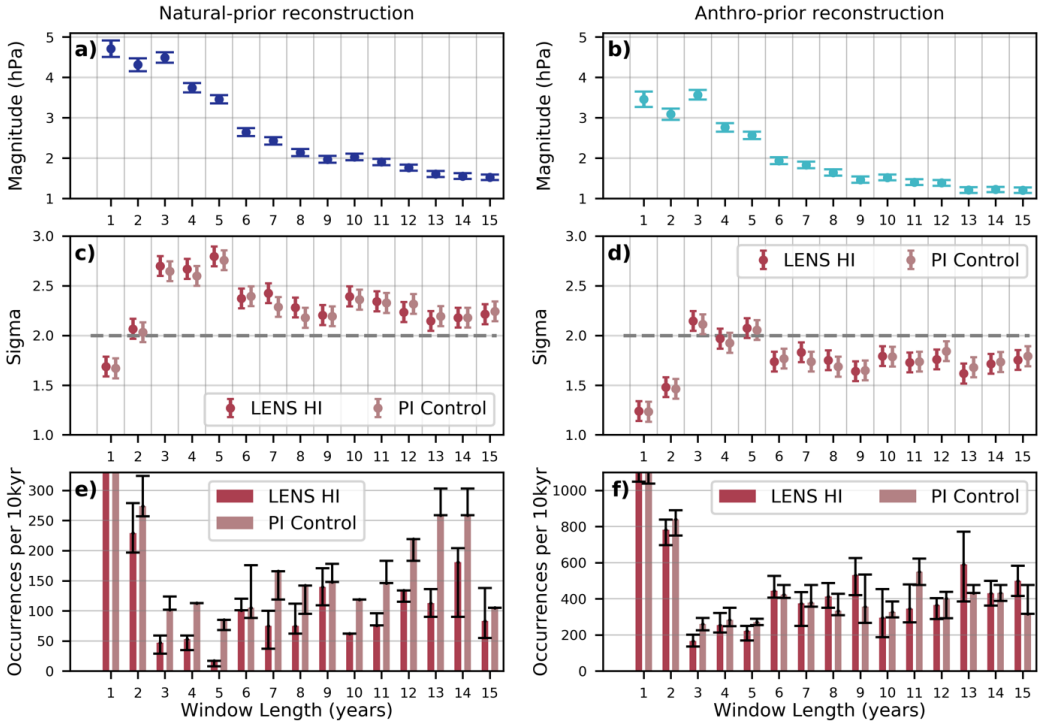

Figure 6. Magnitudes of the 1940s SLP event based on 1-to-15-year averaging windows centered around 1940/41, calculated using (a) the natural-prior reconstruction and the (b) anthro-prior reconstruction (in anomalies relative to 1961 to 1990). The circles represent the mean magnitudes and the error bars represent the 95% confidence intervals. (c, d) Sigma levels of each reconstructed magnitude in panels (a) and (b) relative to two climate model simulations: the Preindustrial Control simulation (PI Control) and the internal component of the LENS Historical simulation (LENS HI). The dashed line highlights the 2-sigma level. (e, f) Histograms of the frequency of the 1940s event based on each averaging window, reported as occurrences per 10kyr (using the magnitudes in (a) and (b)) found in the two climate simulations. The error bars represent occurrences based on the upper and lower bounds of the confidence intervals in (a). The y-axes are selected to highlight the rarest events and differ between (e) and (f); the values for all events can be found in Table 1.

We repeat the magnitude, frequency, and sigma calculations using both reconstructions, corresponding to the left and right columns in Fig. 6. We also repeat the calculation using both sets of climate simulations, corresponding to the two colors in Figs. 6c-f. We use averaging windows between one and fifteen years long centered around the year 1940, allowing us to test the significance of the event in terms of both amplitude and duration (for even numbers, we select 1940.5 as the center value to sit between the different peaks of the event in SLP and Us). These averaging windows correspond to the x-axis on Fig. 6. We note that our overall conclusions are insensitive to the precise choice of center date; for example, they remain unchanged if we instead use 1942 as the end date of the averaging window (which excludes the more negative values in the mid 1940s and includes the more positive values around 1930). Results from the same set of calculations for Us are shown in Fig. 7.

https://doi.org/10.5194/tc-2023-16
Preprint. Discussion started: 21 February 2023

375

4.2 Frequency of the 1940s pressure event

Using the natural-prior reconstruction, the magnitudes and 95% confidence intervals for the 1940s SLP event based on each *x*-year window are shown in Fig. 6a. As expected, the 1 to 3-year windows show the greatest magnitudes, and
380 longer windows show gradually decreasing magnitudes. While the 1-year window shows a similar magnitude to the 2 and 3-year windows, it does not exceed the 2-sigma level relative to internal climate variability; the 2 to 15-year window magnitudes all exceed the 2-sigma level (Fig. 6c). This again demonstrates that the 1940s SLP event is significant because of its combined magnitude and persistence. The absolute number of event occurrences is sensitive to the choice of climate model simulation (LENS HI vs. PI Control), but both simulations show that the 3 to 5-year
385 window magnitudes yield the fewest occurrences (Fig. 6e, Table 1). We estimate ~20 to 50 occurrences per 10ka in the LENS HI simulations and ~90 to 110 occurrences per 10ka in the PI Control simulation (based on the 3 to 5-year mean magnitudes; the lower bounds are ~10 and ~70 occurrences per 10 kyr, respectively). Another local minimum of event occurrences lies at 10 years, which yields ~60 and ~120 occurrences per 10ka in the LENS HI and PI Control simulations, respectively (Table 1).

390

Table 1. Number event occurrences per 10kyr found in the PI Control and LENS HI climate model simulations, based on mean event magnitudes from the natural-prior reconstruction and the anthro-prior reconstruction. The lower bound of occurrences per 10kyr (based on the 95% confidence interval of event magnitudes) is shown in parentheses. The minimum values in each column are bolded. The numbers correspond to the histograms in Figs. 6 and 7.

395

	SLP				**Us**			
	Natural-prior reconstruction		Anthro-prior reconstruction		Natural-prior reconstruction		Anthro-prior reconstruction	
Years in event	LENS HI	PI Control	LENS HI	PI Control	LENS HI	PI Control	LENS HI	PI Control
1	529 (465)	544 (455)	1200 (1049)	1149 (1038)	476 (392)	555 (427)	1162 (988)	1193 (999)
2	229 (197)	274 (257)	782 (697)	840 (750)	76 (58)	72 (56)	370 (300)	352 (302)
3	47 (29)	102 (102)	**166 (136)**	**260 (226)**	53 (47)	68 (45)	375 (297)	487 (374)
4	53 (35)	113 (113)	255 (214)	283 (249)	53 (35)	22 (11)	**250 (184)**	**260 (181)**
5	**17 (8)**	**85 (68)**	223 (169)	272 (255)	35 (8)	**17 (17)**	392 (303)	391 (323)
6	101 (101)	105 (88)	444 (407)	423 (405)	37 (27)	35 (35)	592 (518)	511 (423)
7	75 (37)	166 (119)	375 (250)	380 (357)	75 (25)	23 (23)	625 (487)	666 (595)
8	75 (62)	142 (95)	412 (350)	333 (309)	62 (37)	47 (47)	600 (437)	666 (595)
9	140 (109)	148 (148)	531 (421)	357 (267)	31 (15)	29 (29)	640 (546)	684 (595)
10	62 (62)	119 (119)	296 (187)	327 (297)	**0 (0)**	29 (29)	406 (359)	505 (386)
11	76 (76)	146 (146)	346 (269)	549 (476)	19 (19)	36 (36)	538 (403)	549 (476)
12	134 (115)	219 (183)	365 (288)	402 (293)	**0 (0)**	36 (0)	365 (269)	402 (366)
13	113 (90)	259 (259)	590 (386)	432 (432)	**0 (0)**	43 (43)	454 (431)	606 (476)

https://doi.org/10.5194/tc-2023-16
Preprint. Discussion started: 21 February 2023

14	181 (90)	259 (259)	431 (363)	432 (389)	68 (45)	86 (86)	500 (477)	649 (606)
15	83 (55)	105 (105)	500 (416)	317 (317)	27 (27)	52 (52)	666 (611)	476 (423)

The patterns are similar when we repeat the experiment using the anthro-prior reconstruction, though the significance weakens substantially due to the lower SLP amplitudes (Fig. 6b). In this case, only the 3 and 5-year magnitudes exceed the 2-sigma level (Fig. 6d). The 3 to 5-year magnitudes are again the rarest (Fig. 6f), with ~170 to 260 occurrences per 10kyr using LENS HI, and ~260 to 280 occurrences per 10kyr using PI Control (the lower bounds are ~140 and 230, respectively). This corresponds to ~1 to 3 per century. Another local minimum in the likelihood lies at the 10-year window, yielding ~300 and 330 events per 10 kyr in each model, or ~3 per century (Table 1).

Together, the results from both reconstructions show that the 1940s SLP event is notable in terms of its ~5-year and 10-year means, and that the event is uncommon on centennial timescales but not millennial timescales. We note that the probabilities using the natural-prior SLP reconstruction are more uncertain than those with the anthro-prior reconstruction, as there is greater sensitivity to the choice of simulation used to assess the probability (LENS HI vs. PI Control). The two simulations both reflect internal variability derived from the same native model; the resulting differences in probabilities therefore suggest that the quantification of the externally forced component in the LENS historical ensemble (used to isolate the internal component to produce LENS HI in our analysis) is uncertain, especially for large magnitude SLP events (given that the probability results are more similar when we use the anthro-prior reconstruction, which shows smaller magnitudes). We also note that the anthro-prior SLP reconstruction members have a smaller variance than the simulations and the natural-prior reconstruction members (Fig. 2e), which may partially explain the larger probabilities found using the anthro-prior reconstruction. The true probability of the 1940s SLP event in the ASE shelf break region likely lies between the results from all combinations of reconstructions and climate model simulations: ~20 to 270 occurrences using the 5-year magnitude per 10ka and ~60 to 330 occurrences using the 10-year magnitude per 10ka.

4.3 Frequency of the 1940s zonal wind event

For U_S, we find broadly similar results but with greater sensitivity to the choice of reconstruction, as expected from our earlier analyses. Using the natural-prior reconstruction, we find that the 1 and 2-year windows have the greatest magnitudes. After the 2-year mark, the magnitudes decline as the window size increases (Fig. 7a), and all 2 to 15-year magnitudes exceed the 2-sigma level relative to internal climate variability (Fig. 7c). The sigma level generally increases as the window size increases, until the 10-year mark, after which the significance slightly decreases. Like SLP, the most common U_S magnitude is the 1-year magnitude, which yields ~5 occurrences per century. The 10-year magnitudes yield the rarest frequencies: we estimate 0 and ~30 occurrences per 10 kyr in the LENS HI and PI Control simulations, respectively (Fig. 7e, Table 1). Similar to SLP, the 5-year window lengths yield a local minimum, with ~40 occurrences per 10kyr in LENS HI and ~20 occurrences per 10 kyr in PI Control (based on the mean magnitudes; the lower bounds of the magnitudes yield ~10 and ~20).

https://doi.org/10.5194/tc-2023-16
Preprint. Discussion started: 21 February 2023

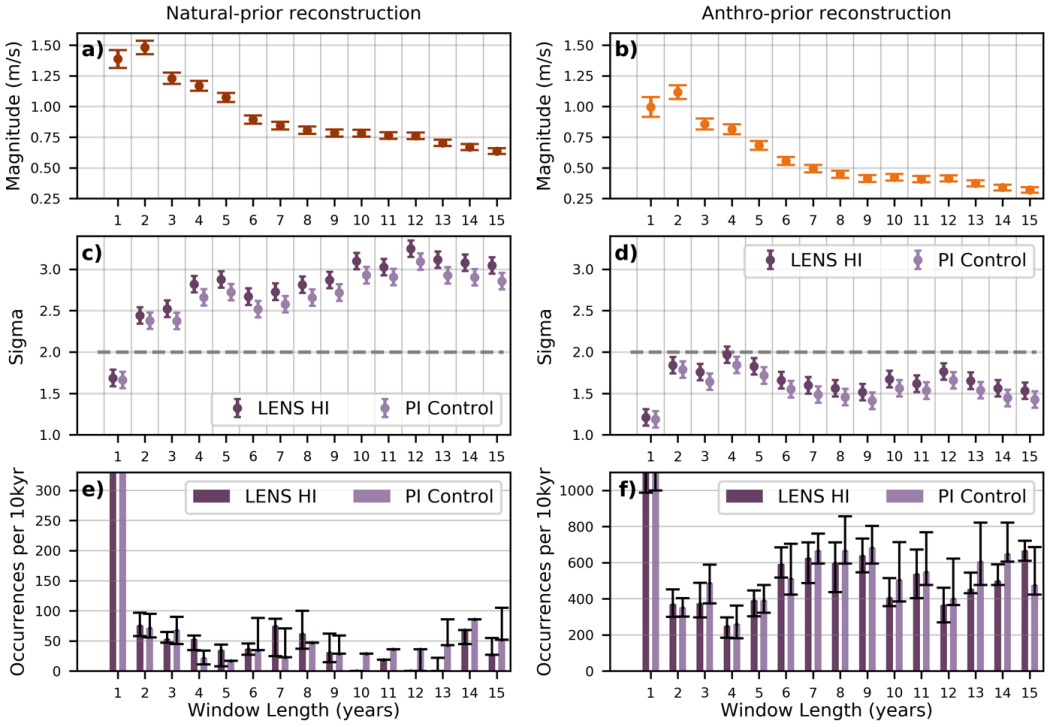

Figure 7. Same as in Fig. 6, but for reconstructions of U_S (geostrophic winds are used for the anthro-prior reconstruction). The values for all events can be found in Table 1.

We repeat this analysis with the anthro-prior geostrophic wind reconstruction, as it has greater skill (*vs.* ERA5) than the directly reconstructed winds (our main conclusions are insensitive to this choice). Again, we find weaker event magnitudes in the anthro-prior reconstruction compared to the natural-prior reconstruction (Fig. 7b), lowering the calculated significance of the events. The 3 to 5-year magnitudes are the most exceptional, but none of the magnitudes exceed the 2-sigma threshold (Fig. 7d). The weaker magnitudes in this reconstruction yield greater event occurrences (Fig. 7f, Table 1). The 1-year magnitude is the most common, yielding ~12 occurrences per century. The 4-year magnitude is the rarest, with ~250 occurrences per 10ka in each set of simulations based on the mean magnitudes, and a lower bound of ~180 occurrences (~2 per century). Again, there is local minimum at the 10-year mark, which yields ~400 and 500 occurrences per 10ka in the LENS HI and PI Control simulations, respectively (~4 and 5 per century).

The results from both reconstructions show that the 1940s U_S event is notable for its combined long duration and large magnitude. We note that the 10-year magnitude comprises approximately half of the amplitude of the shorter window magnitudes (in both the natural-prior and anthro-prior reconstructions), suggesting that the 1940s U_S anomalies may be a result of both interannual variability (i.e., the El Niño event) and interdecadal variability. The calculations for U_S are not hindered by the same uncertainties associated with the SLP analysis: the variances among all datasets are similar (Fig. 2f), and the probabilities are generally less sensitive to the choice of simulation used (LENS HI vs. PI

https://doi.org/10.5194/tc-2023-16
Preprint. Discussion started: 21 February 2023

Control). Therefore, the differences in the probabilities from the natural-prior reconstruction and the anthro-prior reconstruction are a result of the uncertainties in the reconstruction magnitudes (resulting from the different priors used in data assimilation). Using the natural-prior reconstruction, we find evidence that the 1940s U_S event could be significant and even unprecedented on millennial timescales. However, the results from the anthro-prior wind reconstruction do not support this; they instead suggest that the 1940s westerly event is relatively uncommon on centennial timescales and common on millennial timescales. Using all combinations of reconstructions and simulations, the frequency of the 1940s U_S event ranges from ~20 to 400 occurrences per 10 kyr based on its 5-year magnitude, and from ~0 to 500 occurrences per 10ka based on its 10-year magnitude. These values are similar to those for SLP, but with a greater range.

5 Discussion

In this study, the sensitivity to the climate-model prior is especially large for zonal winds, as the difference in reconstructed 20th century wind trends influences the magnitude of the 1940s anomalies (Fig. 1). Anthropogenic forcing may alter the global teleconnection patterns that dictate the information gained from proxy data in the assimilation process, perhaps making the trends in the anthro-prior reconstruction more realistic. However, the skill in the anthro-prior reconstruction (relative to ERA5) is weaker than that of the natural-prior reconstruction, leaving the uncertainties too large to favor the results from either reconstruction in our conclusions.

Our finding that the 1940s event in the ASE is evidently a response to multiple sources of variability highlights the limitations of using datasets constrained by tropical Pacific variability alone (e.g., Holland et al., 2019). While the tropical Pacific is the dominant source of interannual variability in the Amundsen Sea region (Lachlan-Cope and Connolley, 2006; Ding et al., 2011; 2012), other sources of variability can have a substantial impact on large-magnitude events in the ASE. This further illustrates the importance of paleoclimate reconstructions around West Antarctica that include global proxy data, consistent with the findings of Holland et al. (2022), who show that variability arising from regions other than the tropical Pacific can have a large impact on trends in the ASE.

This study is the first to quantify the significance of the 1940s event in the ASE, but our results are associated with several uncertainties as mentioned above. Another caveat is that our analysis focuses only on the shelf-break region. Many previous studies have argued that this is the region most closely associated with the poleward transport of warm CDW (Thoma et al., 2008; Holland et al., 2019; Naughten et al., 2022), and it is close to the spatial peak of the reconstructed 1940s zonal wind anomalies (Fig. 3). However, the relationship between local winds and ocean circulation in this region is complex, as illustrated by regional ocean simulations (e.g., Thoma et al., 2008; Webber et al., 2019; Dotto et al., 2019; Naughten et al., 2022) and oceanographic observations (e.g., Assmann et al., 2013; Wåhlin et al., 2013; Walker et al., 2013; Dutrieux et al., 2014; Kim et al., 2017; Jenkins et al., 2018; Wåhlin et al., 2021). Indeed, recent work suggests that the influence of local shelf-break winds on ocean circulation may change sign on longer timescales (Silvano et al., 2022). Furthermore, large scale atmospheric and oceanic circulation must also

https://doi.org/10.5194/tc-2023-16
Preprint. Discussion started: 21 February 2023

influence CDW transport in the ASE (Nakayama et al., 2018), though the mechanisms related to remote sources of variability have not been comprehensively examined. Finally, we note that we only use simulations from a single native climate model (CESM1) for our probability analysis. We selected this model because it has the least bias in the ASE region, and the reconstructions lie within the range of simulated states (Holland et al., 2019; 2022), but some biases inevitably remain (e.g., in the precise position of the winds).

While our frequency analysis suggests that the 1940s SLP and U_S event is uncommon on centennial timescales and relatively common on millennial timescales, it remains likely that this event played an important role in initiating the current stage of glacier retreat, as suggested by the evidence from sediment cores (Smith et al., 2017). Similar westerly anomalies probably occurred previously during the Holocene, perhaps causing short-lived retreats that the ice recovered from once the atmospheric and associated oceanic perturbation ceased. We propose that the 1940s anomaly may have been the first such event to be superimposed on wider climatic, oceanic, and/or glacial conditions favorable for initiating prolonged retreat (e.g., multi-decadal ocean variability or large-scale warming, or a particularly sensitive ice-sheet grounding line position (Christianson et al., 2016; Jenkins et al., 2018; Christian et al., 2021)). Alternatively, the 1940s event may have caused a similar ice perturbation to previous atmospheric anomalies, but was unusually followed by conditions suitable for ongoing retreat, preventing the ice from recovering from this particular perturbation. For example, anthropogenically forced wind changes driven by greenhouse gas emissions and ozone depletion emerged shortly afterwards, in the latter half of the 20th century (Holland et al., 2022). These hypotheses are consistent with the available evidence but require further investigation.

6 Conclusions

In this study, we use paleoclimate reconstructions and climate model simulations to place novel constraints on the 1940s atmospheric event as a candidate for initiating glacier retreat in the ASE. Using two paleoclimate reconstructions that reflect the range of uncertainty in the available proxy-constrained reconstructions from this time, we find that a large anticyclonic anomaly and strong westerlies occurred in this region with a distinct peak from ~1938-1942, consistent with previous work (Schneider and Steig, 2008). The differences between the reconstructions underscore the importance of considering multiple climate-model priors – and considering anthropogenic forcing – when analyzing reconstructions generated using proxy-data assimilation. The results from our single-proxy experiments and the tropical Pacific pacemaker simulations provide evidence that the event was a combined response to an anomalously persistent El Niño event combined with variability not associated with the tropical Pacific.

In comparison to climate model simulations, the 1940s pressure and zonal wind anomalies are most notable for their combined large magnitude and long duration, with the magnitudes maintained for ~5 years and 10 years being the most significant relative to internal climate variability. Our analysis of the frequency of the 1940s SLP event reveals that it may be as rare as ~20 occurrences per 10 kyr or as common as ~3 occurrences per century; for westerly winds, the frequency ranges from 0 occurrences per 10kyr to ~5 occurrences per century (based on 5 and 10-year means).

https://doi.org/10.5194/tc-2023-16
Preprint. Discussion started: 21 February 2023

These statistics show that the 1940s pressure and zonal wind anomalies are unusual on centennial timescales, but there is insufficient evidence to conclude that they are truly exceptional on millennial timescales. Our results suggest that the 1940s event was probably not unprecedented in the Holocene. However, if the event were superimposed on favorable oceanic or glaciological conditions, or followed by anthropogenically forced trends, the event may have played a role in initiating ice loss. Ocean simulations forced by realistic climate histories, and continued direct observations in the field, are needed to better constrain the mechanisms responsible for glacier retreat in West Antarctica.

Appendix A. Scrambling the reconstruction ensemble members

To generate a scrambled member, we construct the timeseries by randomly drawing a value from the original ensemble for each year. This removes the assumption that each datapoint is autocorrelated in time, serving as a rigorous test for uncertainty. We do this timeseries construction 300 times, producing 300 scrambled reconstruction members. The resulting scrambled ensemble has the same ensemble mean and intra-ensemble variance as the original ensemble for any given year, but the members are now unique realizations (i.e., the gray shaded regions in Fig. 2a and 2c are the same, but the temporal variance in each individual member is different, as annotated on the subpanels). Each scrambled member now has a temporal variance closer to that of the climate model simulations, allowing us to compare the reconstructions to the simulations without major discrepancies in variances (see the variances of all datasets annotated in Fig. 5e/5f). We note that the anthro-prior reconstruction ensemble is slightly smaller in variance than the climate model simulations for SLP, which adds additional uncertainty to our SLP analysis using the anthro-prior reconstruction.

Appendix B. Data processing for the rarity calculation

We take several data processing steps to ensure that the scrambled reconstruction ensembles and climate model simulations are directly comparable. The reconstructions and LENS HI are ensembles that contain members from the period 1920 to 2005. The PI Control simulation is one simulation with 1,801 years, which we split into 86-year-long members to form a similar ensemble (our conclusions are unchanged if we instead concatenate each of the multi-member ensembles into a single long member). To ensure that the anomaly reference periods are handled equally, we remove the mean in each ensemble member from 1961 to 1990 (for the PI Control "ensemble", we remove the mean of the 41st to 70th values in each member). To ensure that all datasets reflect only the internal component of climate variability, we remove the LENS historical ensemble mean time series from the LENS historical ensemble (to form LENS HI) and from the two reconstruction ensembles. The LENS historical ensemble mean time series represents the variability resulting from historical external forcing (Kay et al., 2015). All datasets used for processing and the calculation are shown in Fig. A3.

https://doi.org/10.5194/tc-2023-16
Preprint. Discussion started: 21 February 2023

The Cryosphere
Discussions
Open Access
EGU

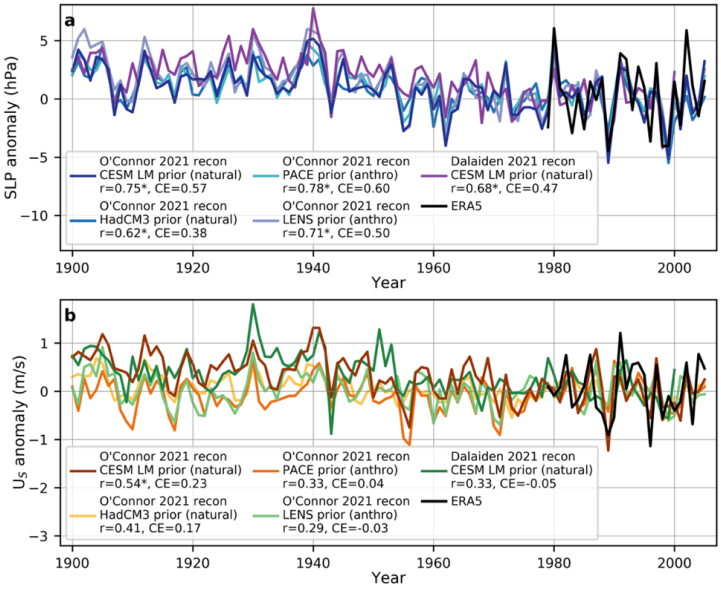

Figure A1. SLP and U_S anomalies in the four reconstructions from O'Connor et al. (2021a), the reconstruction from Dalaiden et al. (2021), and ERA5, all averaged over the ASE continental shelf break box shown in Fig. 2. For each reconstruction, the climate model simulation used as the data assimilation prior (and whether it include natural or anthropogenic forcing) is shown in the legend. The two reconstructions used in this study are the O'Connor et al. (2021a) CESM1 Last Millennium prior reconstruction (referred to as the natural-prior reconstruction) and the PACE prior reconstruction (referred to as the anthro-prior reconstruction). Correlation and CE values compared to ERA5 for the period 1979-2000 are also shown in the legend. The anomaly reference period is 1979-2000 (the period of overlap).

https://doi.org/10.5194/tc-2023-16
Preprint. Discussion started: 21 February 2023

The Cryosphere
Discussions
Open Access
EGU

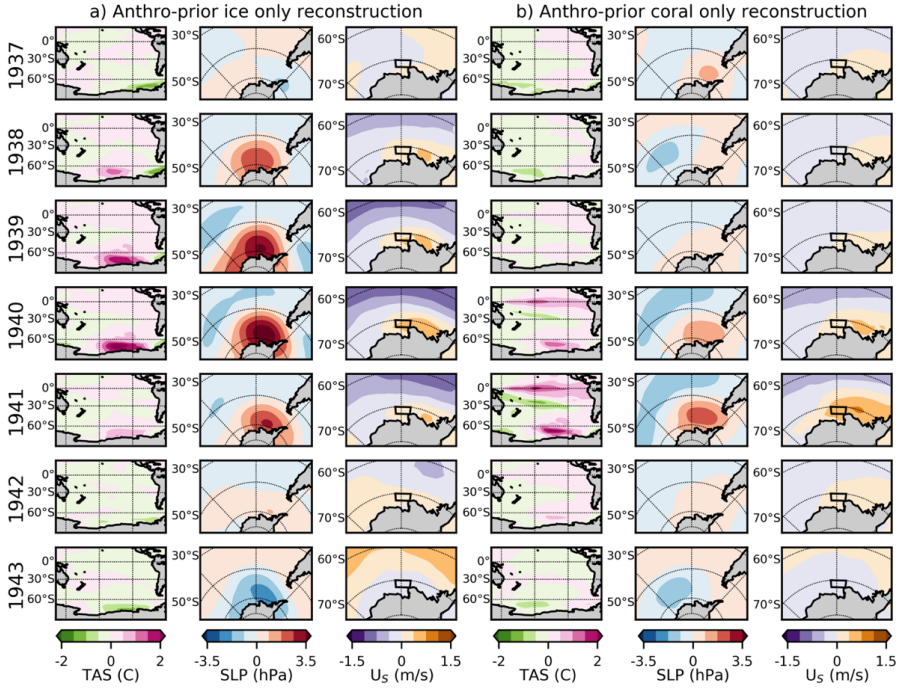

570

Figure A2. Same as in Fig. 4 but using the PACE ensemble as the prior (the anthro-prior).

https://doi.org/10.5194/tc-2023-16
Preprint. Discussion started: 21 February 2023

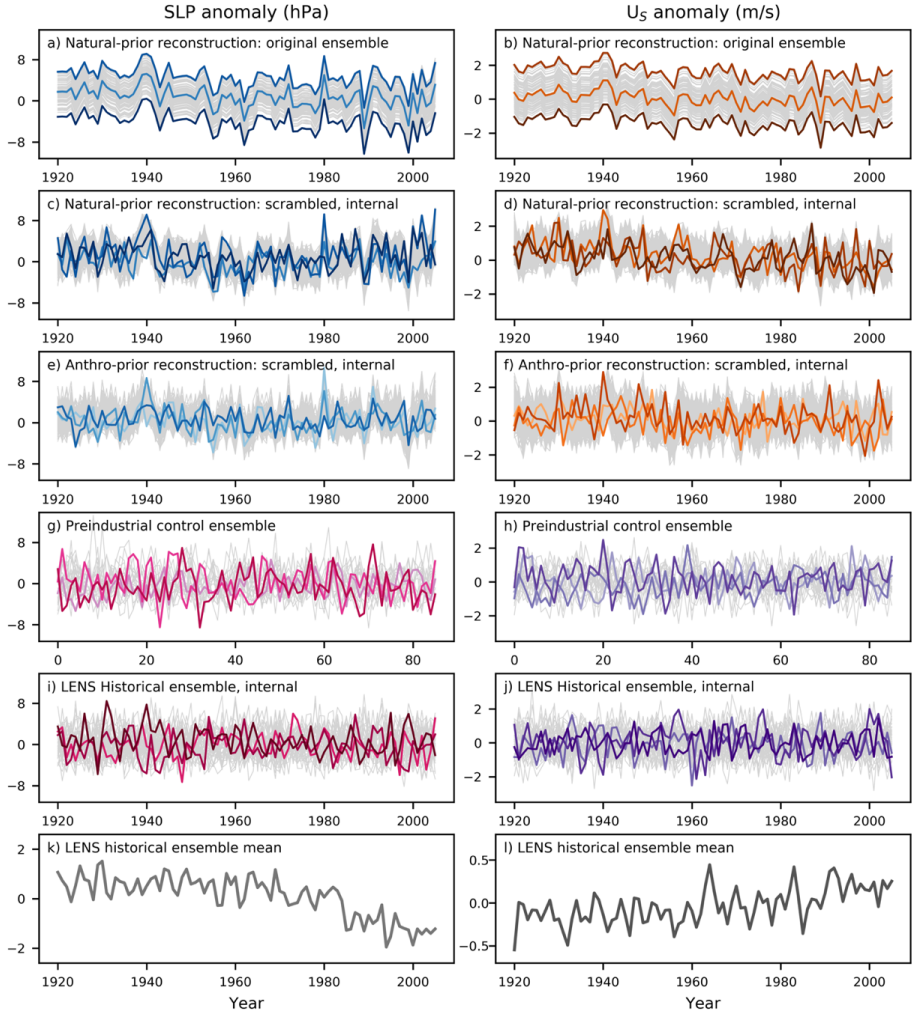

Figure A3. All timeseries used in the calculation of the number of occurrences of the 1940s event for SLP (left column) and U_S (right column): (a, b) the original 100 ensemble members of the natural-prior reconstruction; (c, d) the internal component of the natural-prior reconstruction ensemble, after scrambling the members; (e, f) the internal component of the anthro-prior reconstruction ensemble, after scrambling the members; (g, h) the Preindustrial Control climate model simulation as an ensemble of 86-year-long chunks; (i, j) the internal component of the LENS historical simulation; (k, l) the LENS historical model ensemble mean. All timeseries are in anomalies relative to 1961 to 1990 (or the 41st to 70th values in the Preindustrial Control ensemble). Only three members in each ensemble of data are plotted in color to highlight the variability of each member (the ensemble members containing the minimum, maximum, and median value during 1940 -- or the 20th values in the Preindustrial Control -- are selected); all other members are plotted in gray.

Acknowledgements

https://doi.org/10.5194/tc-2023-16
Preprint. Discussion started: 21 February 2023

G.K.O. was supported by the National Science Foundation Graduate Research Fellowship Program and the University of Washington Peter Misch Fellowship. This study was also partly supported by NSF grants 1602435, 1841844, and 2045075 to E.J.S.

590

Author Contributions

G.K.O, P.R.H, and E.J.S. conceived the study. G.K.O. led the formal analysis and investigation with supervision from P.R.H and E.J.S. All authors contributed to the methodology, interpretation of results, and writing of the manuscript.

595 **Code and Data Availability**

All code used to generate the analysis and figures in this study will be publicly available at https://github.com/goconnor6 prior to publication. The code used to generate the single proxy reconstructions presented here is available at https://github.com/modons/LMR with documentation at https://atmos.washington.edu/~hakim/lmr/docs. The single proxy reconstructions will be archived at Zenodo prior to
600 publication. The other reconstruction data are available at O'Connor et al. (2021a) and Dalaiden et al. (2021). The simulations from CESM1 are available on the NCAR Climate Data Gateway. The ERA5 datasets are available at https://www.ecmwf.int/en/forecasts/datasets.

Competing Interests

605 The authors declare that they have no conflict of interest.

References

Alley, K. E., Wild, C. T., Luckman, A., Scambos, T. A., Truffer, M., Pettit, E. C., Muto, A., Wallin, B., Klinger, M., Sutterly, T.,
610 Child, S. F., Hulen, C., Lenaerts, J. T. M., Maclennan, M., Keenan, E., Dunmire, D.: Two decades of dynamic change and progressive destabilization on the Thwaites Eastern Ice Shelf, The Cryosphere, 15, 5187-5203, 10.5194/tc-15-5187-2021, 2021.

Arblaster, J. M. and Meehl, G. A.: Contributions of external forcings to Southern Annular Mode trends, Journal of Climate, 19, 2896-2905, 10.1175/Jcli3774.1, 2006.

615 Assmann, K. M., Jenkins, A., Shoosmith, D. R., Walker, D. P., Jacobs, S. S., Nicholls, K. W.: Variability of Circumpolar Deep Water transport onto the Amundsen Sea Continental shelf through a shelf break trough, Journal of Geophysical Research Oceans, 118(12), 6603-6620, 2013JC008871, 2013

Bracegirdle, T. J.: Climatology and recent increase of westerly winds over the Amundsen Sea derived from six reanalyses, International Journal of Climatology, 33(4), 843-851, 10.1002/joc.3473, 2013.

620 Bracegirdle, T. J., Turner, J., Hosking, J. S., and Phillips, T.: Sources of uncertainty in projections of 21st century westerly wind changes over the Amundsen Sea, West Antarctica, in CMIP5 climate models., Climate Dynamics, 43, 2093-2104, 10.1007/s00382-013-2032-1, 2014.

Bracegirdle, T. J., Krinner, G., Tonelli, M., Haumann, F. A., Naughten, K. A., Rackow, T., Roach, L. A., and Wainer, I.: Twenty first century changes in Antarctic and Southern Ocean surface climate in CMIP6, Atmospheric Science Letters, 21, e984,
625 10.1002/asl.984, 2020.

Brady, E., Stevenson, S., Bailey, D., Liu, Z., Noone, D., Nusbaumer, J., Otto-Bliesner, B. L., Tabor, C., Tomas, R., Wong, T., Zhang, J., Zhu, J.: The connected isotopic water cycle in the Community Earth System Model Version 1, Journal of Advances in Modeling Earth Systems, 11(8), 2547-2566, 10.1029/2019MS001663, 2019.

Bronnimann, S., Luterbacher, J., Staehelin, J., Svendby, T. M., Hansen, G., Svenoe, T.: Extreme climate of the global troposphere
630 and stratosphere in 1940-42 related to El Niño, Nature, 431, 971-974, 10.1038/nature02982, 2004.

Christian, J. E., Robel, A. A., Catania, G.: A probabilistic framework for quantifying the role of anthropogenic climate change in marine-terminating glacier retreat, The Cryosphere, 16, 2725-2743, 10.5194/tc-16-2725-2022, 2022.

Christianson, K., Bushuk, M., Dutrieux, P., Parizek, B. R., Joughin, I. R., Alley, R. B., Shean, D. E., Abrahamsen, E. P.,

https://doi.org/10.5194/tc-2023-16
Preprint. Discussion started: 21 February 2023

Anandakrishnan, S., Heywood, K. J., Kim, T. W., Lee, S. H., Nicholls, K., Stanton, T., Truffer, M., Webber, B. G. M., Jenkins, A., Jacobs, S., Bindschadler, R., and Holland, D. M.: Sensitivity of Pine Island Glacier to observed ocean forcing, Geophysical Research Letters, 43, 10817-10825, 10.1002/2016gl070500, 2016.

Cobb, K. M.: Coral records of the El Niño-Southern Oscillation and tropical Pacific climate over the last millennium, University of California, 2002.

Dalaiden, Q., Goosse, H., Rezsöhazy, J., and Thomas, E. R.: Reconstructing atmospheric circulation and sea-ice extent in the West Antarctic over the past 200 years using data assimilation, Climate Dynamics, 57, 3479–3503, 10.1007/s00382-021-05879-6, 2021.

Ding, Q. H., Steig, E. J., Battisti, D. S., and Kuttel, M.: Winter warming in West Antarctica caused by central tropical Pacific warming, Nature Geoscience, 4, 398-403, 10.1038/NGEO1129, 2011.

Ding, Q. H., Steig, E. J., Battisti, D. S., and Wallace, J. M.: Influence of the Tropics on the Southern Annular Mode, Journal of Climate, 25(18), 6330-6348,.1175/JCLI-D-11-00523.1, 2012.

Dotto, T. S., Naveira Garabato, A. C., Bacon, S., Holland, P. R., Kimura, S., Firing, Y. L., Tsamados, M., Wahlin, A. K., Jenkins, A.: Wind-driven Processes Controlling Oceanic Heat Delivery to the Amundsen Sea, Antarctica, Journal of Physical Oceanography, 49(11), 2829-2849, 10.1175/JPO-D-19-0064.1, 2019

Dutrieux, P., De Rydt, J., Jenkins, A., Holland, P. R., Ha, H. K., Lee, S. H., Steig, E. J., Ding, Q. H., Abrahamsen, E. P., and Schroder, M.: Strong Sensitivity of Pine Island Ice-Shelf Melting to Climatic Variability, Science, 343, 174-178, 10.1126/science.1244341, 2014.

Fogt, R. L., Schneider, D. P., Goergens, C. A., Jones, J. M., Clark, L. N., and Garberoglio, M. J.: Seasonal Antarctic pressure variability during the twentieth century from spatially complete reconstructions and CAM5 simulations, Climate Dynamics, 53, 1435–1452, 10.1007/s00382-019-04674-8, 2019.

Goyal, R., Gupda, A. S., Jucker, M., and England, M. H.: Historical and projected changes in the Southern Hemisphere surface westerlies., Geophysical Research Letters, 48, e2020GL090849, 10.1029/2020GL090849, 2021.

Hakim, G. J., Emile-Geay, J., Steig, E. J., Noone, D., Anderson, D. M., Tardif, R., Steiger, N., and Perkins, W. A.: The last millennium climate reanalysis project: Framework and first results, Journal of Geophysical Research - Atmospheres, 121, 6745-6764, 10.1002/2016JD024751, 2016.

Hersbach, H.: The ERA5 global reanalysis, Quarterly Journal of the Royal Meteorological Society, 146, 1999-2049, 10.1002/qj.3803, 2020.

Holland, P. R., Bracegirdle, T. J., Dutrieux, P., Jenkins, A., and Steig, E. J.: West Antarctic ice loss influenced by internal climate variability and anthropogenic forcing, Nature Geoscience, 12, 718-724, 10.1038/s41561-019-0420-9, 2019.

Holland, P. R., O'Connor, G. K., Bracegirdle, T. J., Dutrieux, P., Naughten, K. A., Steig, E. J., Schneider, D. P., Jenkins, A., Smith, J. A.: Anthropogenic and internal drivers of wind changes over the Amundsen Sea, West Antarctica during the 20th and 21st centuries, The Cryosphere, 16, 5085-5105, 10.5194/tc-16-5085-2022, 2022.

Huang, B., Thorne, P. W., Banzon, V. F., Boyer, T., Chepurin, G., Lawrimore, J. H., Menne, M. J., Smith, T. M., Vose, R. S., and Zhang, H. M.: Extended reconstructed sea surface Temperature version 5 (ERSSTv5), upgrades, validations, and intercomparisons, Journal of Climate, 30(20), 8179–8205, 10.1175/JCLI-D-16-0836.1, 2017.

Jenkins, A., Dutrieux, P., Jacobs, S. S., Steig, E. J., Gudmundsson, G. H., Smith, J., & Heywood, K. J.: Decadal ocean forcing and Antarctic Ice Sheet response: Lessons from the Amundsen Sea. Oceanography, 29(4), 106–117. 10.5670/oceanog.2016.103, 2016.

Jenkins, A., Shoosmith, D., Dutrieux, P., Jacobs, S., Kim, T. W., Lee, S. H., Ha, H. K., Stammerhohn, S.: West Antarctic Ice Sheet retreat in the Amundsen Sea driven by decadal oceanic variability, Nature Geoscience, 11, 733-738, 10.1038/s41561-018-0207-4, 2018.

Kay, J. E., Deser, C., Phillips, A., Mai, A., Hannay, C., Strand, G., Arblaster, J. M., Bates, S. C., Danabasoglu, G., Edwards, J., Holland, M., Kushner, P., Lamarque, J. F., Lawrence, D., Lindsay, K., Middleton, A., Munoz, E., Neale, R., Oleson, K., Polvani, L., and Vertenstein, M.: The Community Earth System Model (CESM) Large Ensemble Project: A Community Resource for Studying Climate Change in the Presence of Internal Climate Variability, Bulletin of the American Meteorological Society, 96, 1333-1349, 10.1175/Bams-D-13-00255.1, 2015.

Kim, T. W., Ha, H. K., Wahlin, A. K., Lee, S. H., Kim, C. S., Lee, J. H., Cho, Y. K.: Is Ekamn pumping responsible for the seasonal variation of warm circumpolar deep water in the Amundsen Sea?, Continental Shelf Research, 132(1), 38-48, 10.1016/j.csr.2016.09.005, 2017.

Lachlan-Cope, T. and Connolley, W.: Teleconnections between the tropical Pacific and the Amundsen-Bellinghausens sea: Role of the El Niño Southern Oscillation, Journal of Geophysical Research-Atmospheres, 111, D23101, 10.1029/2005jd006386, 2006.

Larter, R. D., Anderson, J. B., Graham, A. G. C., Gohl, K., Hillenbrand, C.-D., Jakobsson, M., Johnson, J. S., Kuhn, G., Nitsche, F., Smith, J. A., Witus, A. E., Bentley, M. J., Dowdeswell, J. A., Ehrmann, W., Klages, J. P., Lindow, J., O Cofaigh, C., and Spiegel, C.: Reconstruction of changes in the Amundsen Sea and Bellingshausen Sea sector of the West Antarctic Ice Sheet since the Last Glacial Maximum, Quaternary Science Reviews, 100, 55-86, 10.1016/j.quascirev.2013.10.016, 2014.

Li, X., Cai, W., Meehl, G.A., Chen, D., Yuan, X., Raphael, M., Holland, D.M., Ding, Q., Fogt, R.L., Markle, B.R., Wang, G., et al.: Tropical teleconnection impacts on Antarctic climate changes, Nature Reviews Earth & Environment, 2(10), 680-698, 10.1038/s43017-021-00204-5, 2021.

Naughten, K. A., Holland, P. R., Dutrieux, P., Kimura, S., Bett, D. T., and Jenkins, A.: Simulated twentieth-century ocean

https://doi.org/10.5194/tc-2023-16
Preprint. Discussion started: 21 February 2023

warming in the Amundsen Sea, West Antarctica, Geophysical Research Letters, 49, e2021GL094566, 10.1029/2021GL094566, 2022.

Nakayama, Y., Menemenlis, D., Zhang, H., Schodlok, M., and Rignot, E.: Origin of Circumpolar Deep Water intruding onto the Amundsen and Bellingshausen Sea continental shelves, Nature Communications, 9(1), 3403, 10.1038/s41467-018-05813-1, 2018.

O'Connor, G. K., Steig, E. J., and Hakim, G. J.: Strengthening Southern Hemisphere westerlies and Amundsen Sea Low deepening over the 20th century revealed by proxy-data assimilation, Geophysical Research Letters, 48, e2021GL095999, 10.1029/2021GL095999, 2021a.

O'Connor, G. K., Cobb, K. M., Sayani, H. R., Atwood, A. R., Grothe, P. R., Stevenson, S., Baum, J. K., Chen, T., Claar, D. C., Hitt, N. T., Lynch-Stieglitz, J., Mortlock, R. A., Schmidt, G. A., Walter, R.: Coral Oxygen Isotopic Records Capture the 2015/2016 El Niño Event in the Central Equatorial Pacific, Geophysical Research Letters, 48(24), e2021GL094036, 0.1029/2021GL094036, 2021b.

Okumura, Y. M., Schneider, D., Deser, C., and Wilson, R.: Decadal-interdecadal climate variability over Antarctica and linkages to the tropics: Analysis of ice core, instrumental, and tropical proxy data, Journal Of Climate, 25, 7421-7441, 10.1175/JCLI-D-12-00050.1, 2012.

PAGES2k Consortium: A global multiproxy database for temperature reconstructions of the Common Era, Scientific Data, 4, 170088, 10.1038/sdata.2017.88, 2017.

Pritchard, H. D., Ligtenberg, S. R. M., Fricker, H. A., Vaughn, D. G., van den Broeke, M. R., and Padman, L.: Antarctic ice-sheet loss driven by basal melting of ice shelves. Nature, 484, 502–505, 10.1038/nature10968, 2012.

Sanchez, S. C., Westphal, N., Haug, G. H., Cheng, H., Edwards, R. L., Schneider, T., Cobb, K. M., Charles, C. D.: A Continuous Record of Central Tropical Pacific Climate Since the Midnineteenth Century Reconstructed From Fanning and Palmyra Island Corals: A Case Study in Coral Data Reanalysis, Paleoceanography and Paleoclimatology, 35(8), e2020PA003848, 10.1029/2020PA003848, 2020.

Sanchez, S. C., Hakim, G. J., and Saenger, C. P.: Climate model teleconnection patterns govern the Niño 3.4 response to early 19th century volcanism in coral-based data assimilation reconstructions. Journal of Climate, 34(5), 1863–1880, 10.1175/JCLI-D-20-0549.1, 2021.

Schneider, D. P. and Deser, C.: Tropically driven and externally forced patterns of Antarctic sea ice change: reconciling observed and modeled trends, Climate Dynamics, 50, 4599-4618, 10.1007/s00382-017-3893-5, 2018.

Schneider, D. P. and Steig, E. J.: Ice cores record significant 1940s Antarctic warmth related to tropical climate variability, Proceedings of the National Academy of Sciences of the United States of America, 105, 12154-12158, 10.1073/pnas.0803627105, 2008.

Shepherd, A., Gilbert, L., Muir, A. S., Konrad, H., McMillan, M., Slater, T., Briggs, K. H., Sundal, A. V., Hogg, A. E., and Engdahl, M. E.: Trends in Antarctic Ice Sheet Elevation and Mass, Geophysical Research Letters, 46, 8174-8183, 10.1029/2019gl082182, 2019.

Silvano, A., Holland, P. R., Naughten, K. A., Dragomir, O., Dutrieux, P., Jenkins, A., Si, Y., Stewart, A. L., Peña Molino, B., Janzing, G. W., Dotto, T. S., Naveira Garabato, A. C.: Baroclinic ocean response to climate forcing regulates decadal variability of ice-shelf melting in the Amundsen Sea, Geophysical Research Letters, 49, e2022GL100646, 10.1029/2022GL100646, 2022.

Slivinski, L. C., Compo, G. P., Whitaker, J. S., Sardeshmukh, P. D., Giese, B. S., McColl, C., Allan, R., Yin, X., Vose, R., Titchner, H., Kennedy, J., Spencer, L.J., Ashcroft, L., Brönnimann, S., Brunet, M., Camuffo, D., Cornes, R., Cram, T.A., Crouthamel, R., Domínguez-Castro, F., Freeman, J. E., Gergis, J., Hawkins, E., Jones, P.D., Jourdain, S., Kaplan, A., Kubota, H., Blancq, F. L., Lee, T., Lorrey, A., Luterbacher, J., Maugeri, M., Mock, C. J., Moore, G. W. K., Przybylak, R., Pudmenzky, C., Reason, C., Slonosky, V. C., Smith, C. A., Tinz, B., Trewin, B., Valente, M. A., Wang, X. L., Wilkinson, C., Wood, K., and Wyszyński, P.: Towards a more reliable historical reanalysis: Improvements for version 3 of the Twentieth Century Reanalysis system, Q. J. Roy. Meteor. Soc., 145, 2876–2908, 10.1002/qj.3598, 2019.

Smith, J. A., Andersen, T. J., Shortt, M., Gaffney, A. M., Truffer, M., Stanton, T. P., Bindschadler, R., Dutrieux, P., Jenkins, A., Hillenbrand, C. D., Ehrmann, W., Corr, H. F. J., Farley, N., Crowhurst, S., and Vaughan, D. G.: Sub-ice-shelf sediments record history of twentieth-century retreat of Pine Island Glacier, Nature, 549, 292-292, 10.1038/nature23650, 2017.

Smith, B., Fricker, H. A., Gardner, A. S., Medley, B., Nilsson, J., Paolo Nicholas Holschuh, F. S., Adusumilli, S., Brunt, K., Csatho, B., Harbeck, K., Markus, T., Neumann, T., Siegfried, M. R., and Jay Zwally, H.: Pervasive ice sheet mass loss reflects competing ocean and atmosphere processes, Science, 368, 1239–1242, 10.1126/science.aaz5845, 2020.

Steig, E.J., Mayewski, P.A., Dixon, D., Kaspari, S, Frey, M., Schneider, D., Arcone, S., Hamilton, G., Spikes, V., Albert, M., Mess, D., Gow, A., Shuman, C. White, J.W.C., Sneed, S., Flaherty, J., and Wumkes, M.: High-resolution Ice Cores from US ITASE (West Antarctica): development and validation of chronologies and determination of precision and accuracy, Annals of Glaciology, 41, 77-84, 10.3189/17275640578181331, 2005.

Steig, E. J., Ding, Q., Battisti, D. S., and Jenkins, A.: Tropical forcing of Circumpolar Deep Water Inflow and outlet glacier thinning in the Amundsen Sea Embayment, West Antarctica, Annals of Glaciology, 53, 19-28, 10.3189/2012AoG60A110, 2012.

Steig, E. J., Ding, Q. H., White, J. W. C., Kuttel, M., Rupper, S. B., Neumann, T. A., Neff, P. D., Gallant, A. J. E., Mayewski, P.

https://doi.org/10.5194/tc-2023-16
Preprint. Discussion started: 21 February 2023

A., Taylor, K. C., Hoffmann, G., Dixon, D. A., Schoenemann, S. W., Markle, B. R., Fudge, T. J., Schneider, D. P., Schauer, A. J., Teel, R. P., Vaughn, B. H., Burgener, L., Williams, J., and Korotkikh, E.: Recent climate and ice-sheet changes in West Antarctica compared with the past 2,000 years, Nature Geoscience, 6, 372-375, 10.1038/Ngeo1778, 2013.

Thoma, M., Jenkins, A., Holland, D., and Jacobs, S.: Modelling Circumpolar Deep Water intrusions on the Amundsen Sea continental shelf, Antarctica, Geophysical Research Letters, 35, L18602, 10.1029/2008gl034939, 2008.

Thomas, E. R., Melchior Van Wessem, J., Roberts, J., Isaksson, E., Schlosser, E., Fudge, T. J., Vallelonga, P., Medley, B., Lenaerts, J., Bertler, N., Van Den Broeke, M. R., Dixon, D. A., Frezzotti, M., Stenni, B., Curran, M., Ekaykin, A. A.: Regional Antarctic snow accumulation over the past 1000 years, Climate of the Past, 13(11):1491–1513, 10.5194/cp-13-1491-2017, 2017.

Thompson, D. W. J., Solomon, S., Kushner, P. J., England, M. H., Grise, K. M., and Karoly, D. J.: Signatures of the Antarctic ozone hole in Southern Hemisphere surface climate change, Nature Geoscience, 4, 741-749, 10.1038/Ngeo1296, 2011.

Wåhlin, A. K., Kalen, O., Arneborg, L., Bjork, G., Carvajal, G. K., Ha, H. K., Kim, T. W., Lee, S. H., Lee, J. H., Stranne, C.: Variability of Warm Deep Water Inflow in a Submarine Trough on the Amundsen Sea Shelf, Journal of Physical Oceanography, 43(10), 2054-2079, 2013.

Wåhlin, A. K., Graham, A. G. C., Hogan, K. A., Queste, B. Y., Boehme, L., Larter, R. D., Pettit, E. C., Wellner, J., Heywood, K. J.: Pathways and modification of warm water flowing beneath Thwaites Ice Shelf, West Antarctica, Science Advances, 7(15), eabd7254, 10.1175/JPO-D-12-0157.1, 2021.

Walker, D. P., Jenkins, A. Assmann, K. M., Shoosmith, D. R., Brandon, M. A.: Oceanographic observations at the shelf break of the Amundsen Sea, Antarctica, Journal of Geophysical Research Oceans, 118(6), 2906-2918, 10.1002/jgrc.20212, 2013.

Webber, B. G. M., Heywood, K. J., Stevens, D. P., Assmann, K. M.: The Impact of Overturning and Horizontal Circulation in Pine Island Trough on Ice Shelf Melt in the Eastern Amundsen Sea, Journal of Physical Oceanography, 49(1), 63-83, 10.1175/JPO-D-17-0213.1, 2019.

Wohland, J., Omrani, N. E., Witthaut, D., and Keenlyside, N. S.: Inconsistent wind speed trends in current twentieth century reanalyses, Journal of Geophysical Research: Atmospheres, 124, 1931–1940, 10.1029/2018JD030083, 2019.